R-matrix propagation with adiabatic bases for the photoionization spectra of atoms in magnetic fields

F. Mota-Furtado* and P. F. O'Mahony†
Department of Mathematics, Royal Holloway, University of London, Egham, Surrey TW20 0EX, United Kingdom
(Received 27 August 2007; published 8 November 2007)

The photoionization spectrum of an atom in a magnetic field is calculated by combining *R*-matrix propagation with local adiabatic basis expansions. This approach considerably increases the speed and the energy range over which calculations can be performed compared to previous methods, allowing one to obtain accurate partial and total cross sections over an extended energy range for an arbitrary magnetic field strength. In addition, the cross sections for all atoms of interest can be calculated simultaneously in a single calculation. Multichannel quantum defect theory allows for a detailed analysis of the resonance structure in the continuum. Calculated cross sections for a range of atoms at both laboratory and astrophysical field strengths are presented.

DOI: 10.1103/PhysRevA.76.053405 PACS number(s): 32.60.+i, 32.80.Fb, 95.30.Ky

I. INTRODUCTION

The spectrum of an atom in a magnetic field has played an important role in the development of quantum theory and in atomic structure [1]. For a long time, the effect of the external field on the atom was treated perturbatively. However, with the discovery of large magnetic fields in white dwarf (10^2–10^5 T) and neutron stars (10^7–10^9 T) in the 1970s, attention has focused on nonperturbative treatments of the field-atom interaction [2]. For laboratory strength magnetic fields (6 T), the potential due to the applied field becomes comparable to the intrinsic Coulomb potential only for an electron in a high Rydberg state or continuum state of the atom. In the 1980s and 1990s, research was focused on atoms in laboratory strength fields, as these systems have an inherent nonseparability arising from the competing spherical symmetry of the atom and the cylindrical symmetry of the applied field, which leads to the classical system exhibiting chaotic behavior [3]. An atom in a field thus provides an experimentally realizable quantum system whose corresponding classical phase space is chaotic, serving as a prototype for studying classical and quantum chaos. This led to fruitful developments in the theory of quantum chaos [4].

For bound states of atoms in a magnetic field, large-scale basis set calculations have proved very successful in finding the energy eigenstates and photoabsorbtion spectra of atoms in moderately strong fields [2]. For superstrong fields such as those found in neutron stars, the field can modify the atomic structure of the ground state of the atom, and different theoretical techniques have to be used. Currently, for these cases, the energy eigenstates and photoabsorbtion spectra are known for only some low levels of a few light atoms [5].

The positive-energy or continuum spectra of an atom in a field proved more challenging, particularly in calculating photoionization cross sections at laboratory strength fields. The three main theoretical methods that have been successful at calculating cross sections at both laboratory and astrophysical strength fields are the complex coordinate method of Delande *et al.* [6], the *R*-matrix method of O'Mahony and Mota-Furtado [7,8], and the diabatic by-sector method of Watanabe and Komine [9]. A detailed comparison between theory and experiment was possible due to the high-resolution experiments carried out by Iu *et al.* [10] on lithium in a field of about 6 T. Although all three approaches have recreated the experimental spectrum of Iu *et al.* over a narrow energy region, they are not particularly suited to calculating the photoionization spectrum over a large energy region. We present here a major improvement on previous *R*-matrix methods applied to this problem by using local adiabatic basis states to propagate the *R*-matrix from low *r* to the asymptotic region. This leads to a large saving in both the CPU time and computer memory required to perform the calculation. In addition, for a given value of the field strength, the cross sections for all atoms of interest can be calculated in one step without the need for any additional propagations. We demonstrate that, by using a combination of *R*-matrix propagation with local adiabatic basis states and multichannel quantum defect theory (MQDT) [11] one has a method that can be used to calculate photoionization cross sections of any atom over very large energy regions and field strengths. MQDT can also be used to analyze the resonance structure in detail where, in general, several Rydberg series interact with a set of complex short-range perturbers. An efficient approach to calculating such cross sections is of importance in many areas where magnetic fields play a role, for example, in calculating stellar opacities for magnetic white dwarfs or for evaluating recombination rates for an atom or ion in a magnetic field at low temperatures (e.g., antihydrogen), where one has to calculate the cross section over very large energy regions for a given field strength.

In Sec. II we give the theory used to evaluate the photoionization cross section of an atom in an external magnetic field by combining *R*-matrix propagation with local adiabatic basis states and MQDT. In Sec. III all the required details of the computation are given. The results of the calculations are presented in Sec. IV for a variety of atoms at both laboratory and astrophysical field strengths, and a conclusion is given in Sec. V. In the Appendix we give details on how to construct the Hamiltonian matrix for the propagation.

*f.motafurtado@rhul.ac.uk
†p.omahony@rhul.ac.uk

II. THEORY

The Hamiltonian for a hydrogen atom in a magnetic field (taken to be in the z direction) in the symmetric gauge can be written using atomic units ($\hbar=m=e=1$) as [1]

$$H=-\frac{\nabla^2}{2}-\frac{1}{r}+\beta L_z+\frac{1}{2}\beta^2 r^2\sin^2\theta \tag{1}$$

where the magnetic field B is measured in atomic units by $\beta=B/B_0$ with $B_0=4.701\,08\times10^5$ T. (We neglect the spin as it only produces a uniform shift in the energy scale.) The Hamiltonian has two conserved quantities in addition to the energy, namely, the z component of the angular momentum L_z and π_z, the z parity. The eigensolutions can thus be studied for fixed values of m, the azimuthal quantum number, and for $\pi_z=\pm1$. The linear Zeeman term in Eq. (1) thus adds only a uniform shift to the total energy.

When a photon excites an electron to the continuum, for a given magnetic field strength, one can in general identify three regions of interaction with the continuum electron [8]. Typically, for low r the spherically symmetric Coulomb potential dominates over the cylindrically symmetric diamagnetic term or the quadratic term in Eq. (1), at intermediate values of r the Coulomb and magnetic potentials are of comparable strength (the strong-mixing region), and at high values of r or asymptotically in r the cylindrical symmetry of the diamagnetic potential predominates. For a general atom (or molecule) one adds a fourth region, the core, where the excited electron interacts with the multielectron core before emerging into the Coulomb region described by the Hamiltonian in Eq. (1). Exploiting this natural partition in configuration space forms the basis of the R-matrix approach to solving atomic and molecular problems, where solutions are sought in each region and then matched together at the boundaries between the regions to form the solution over all space [12]. A novel aspect of the magnetic field problem is having to deal with the change in symmetry from spherical to cylindrical, which involves introducing two-dimensional matching procedures [8]. We describe below how the R-matrix is propagated through the regions described above and how the two-dimensional matching procedure is implemented to give the reactance matrix and the photoionization cross section.

A. Propagating the R matrix

An atom in a magnetic field is assumed to be excited from an initial state, either a ground or low-lying excited state, by a polarized photon, leading to an electron in the continuum with specific values of m and π_z. The electron emerges from the first region, the core region, into the second or Coulomb region with energy ϵ where Eq. (1) can be approximated by the field-free Hamiltonian because the diamagnetic terms are negligible in comparison with those from the Coulomb potential of the atomic core. [We shall assume here that the field strengths for nonhydrogenic atoms are not large enough to significantly distort the core (i.e., $\beta<1$). For $\beta>1$ a different treatment would be required for the core, although the propagation outside the core could still be implemented.] Therefore, at some radius $r=a$ in the Coulomb region, the radial form of the lth partial wave of the wave function, $F_l^\epsilon(r)$, of the continuum electron can be written in terms of a linear combination of the energy-normalized regular s and irregular c Coulomb functions [13] in spherical coordinates or a phase-shifted Coulomb function, giving the general form of the solution as

$$\begin{aligned}\Psi_\epsilon&=\sum_l F_l^\epsilon(r)Y_{lm}(\theta,\phi)\\&=\sum_l A_l^\epsilon[s_l^\epsilon(r)+c_l^\epsilon(r)\tan(\pi\mu_l)]Y_{lm}(\theta,\phi),\end{aligned} \tag{2}$$

where the A_l^ϵ are constants to be determined and $Y_{lm}(\theta,\phi)$ are the spherical harmonics. The quantum defects μ_l represent the effects of the nonhydrogenic field-free core [11] and can be calculated *ab initio* or taken from experiment. [For the most general case, where the ionic core could be left in different excited states, a coupled multichannel solution would be appropriate at $r=a$ with $\tan(\pi\mu_l)$ being replaced by a reactance matrix. This is a straightforward generalization of the method.] Knowing the phase-shifted Coulomb function and its derivative at $r=a$, the R matrix [12] or log-derivative can be constructed on the outer boundary of this region as

$$\begin{aligned}R_{ll'}=[s_l^\epsilon(a)+c_l^\epsilon(a)\tan(\pi\mu_l)]\Bigg(&\frac{d}{dr}[s_l^\epsilon(r)\\&+c_l^\epsilon(r)\tan(\pi\mu_l)]\Bigg|_{r=a}\Bigg)^{-1}\delta_{ll'},\end{aligned} \tag{3}$$

since the coefficients A_l^ϵ cancel out in the above expression.

In the third or strong-mixing region the effects due to the Coulomb potential of the core and those due to the magnetic field are of a comparable size. This region is defined by $a<r<b$ where the radius b is taken to be large enough such that the Hamiltonian is separable in cylindrical coordinates. The change in symmetry of the potential, from spherical to cylindrical, is therefore completely contained within this region. We wish to propagate the initial R matrix in Eq. (3) to obtain the R matrix at the outer boundary of this region $r=b$ [14,15]. To do this we divide the region into N radial sectors with radii $a\rightarrow a_1$, $a_1\rightarrow a_2,\ldots,$ $a_{N-1}\rightarrow b$. The size of each sector and the number of sectors N are important parameters in the calculation, and we show later how these are optimally determined. Within each of the sectors we construct a local adiabatic basis as follows. For the nth sector we take a radius r_a^n within the sector $a_{n-1}<r_a^n<a_n$, which is usually the midpoint of the sector, and we diagonalize the fixed r or adiabatic Hamiltonian H_{ad}

$$H_{ad}(r_a^n;\theta,\phi)=\frac{\mathbf{L}^2}{2(r_a^n)^2}-\frac{1}{r_a^n}+\frac{1}{2}\beta^2(r_a^n)^2\sin^2\theta \tag{4}$$

in a basis set of spherical harmonics such that

$$\phi_\lambda(r_a^n;\theta,\phi)=\sum_l d_{l\lambda}Y_{lm}(\theta,\phi), \tag{5}$$

where the $d_{l\lambda}$ are constants, giving the eigenvalue equation

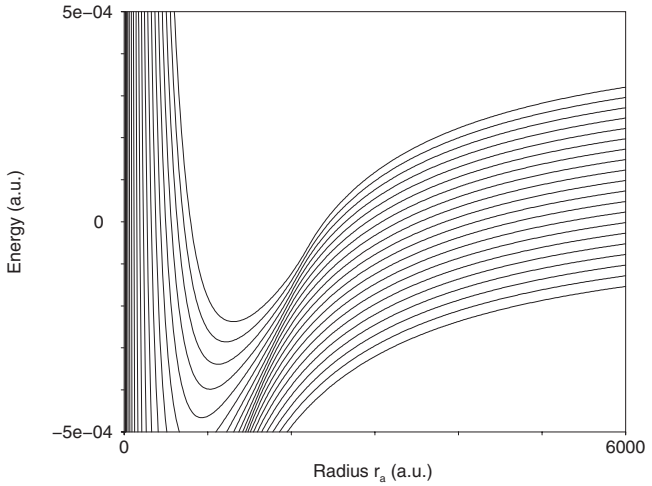

FIG. 1. First 20 adiabatic eigenvalue curves obtained from diagonalizing the adiabatic Hamiltonian H_{ad} in a basis set of spherical harmonics at successive r. The magnetic field strength used was 6 T. The centrifugal barrier can be seen at small r and the Coulomb potential plus equal Landau spacing is seen as $r\to\infty$. There is a set of avoided crossings in between.

$$H_{ad}\phi_\lambda = U_\lambda(r_a^n)\phi_\lambda. \tag{6}$$

The adiabatic states form a locally optimized basis set for each sector. An adiabatic set of potential curves can be produced by plotting the eigenvalues obtained from diagonalizations at a continuous set of successive values of r. A typical set of curves is shown in Fig. 1. At small r the adiabatic eigenfunctions are spherical harmonics and the potential exhibits a centrifugal barrier. At large r these curves have the equal energy spacing of Landau states (combined with the $-1/r$ falloff), and the eigenfunctions are localized in the cylindrical coordinates ρ and ϕ. The change in symmetry happens predominantly around a region of avoided crossings that can clearly be seen in the diagram. The functions ϕ_λ are therefore a very good basis with which to represent the angular part of the wave function in the local region around r_a^n, namely, within the sector n.

To propagate the R matrix from sector to sector, we use these basis states within each sector and diagonalize the full Hamiltonian [Eq. (1)] plus the Bloch operator L or surface term [16],

$$L = \frac{1}{2}\left(\delta(r-a_n)\frac{d}{dr} - \delta(r-a_{n-1})\frac{d}{dr}\right), \tag{7}$$

in a basis set consisting of a product of orthogonal radial functions $f_j(r)$ and the adiabatic functions generated for that sector, $\phi_\lambda(r_a^n;\theta,\phi)$. The radial basis functions used are defined in terms of Legendre polynomials P_j as follows [15]:

$$f_j(r) = \sqrt{\frac{2j-1}{a_n - a_{n-1}}}P_{j-1}(u), \tag{8}$$

where

$$u = \frac{2}{a_n - a_{n-1}}\left[r - \left(\frac{a_n + a_{n-1}}{2}\right)\right].$$

The eigenvalue equation is thus

$$(H+L)\Psi^k = E_k\Psi^k. \tag{9}$$

The eigenfunctions obtained from diagonalizing this operator are therefore

$$\Psi^k = \sum_{j\lambda} c_{j\lambda}^k \frac{f_j(r)}{r}\phi_\lambda(r_a^n;\theta,\phi). \tag{10}$$

The total continuum wave function at any energy ϵ, Ψ_ϵ, can be expanded in terms of these R-matrix eigenstates Ψ^k. Since the general solution in the nth sector can also be written as $\Psi_\epsilon = \Sigma_\lambda F_\lambda(r)\phi_\lambda(r_a^n;\theta,\phi)$ it is straightforward to show [15], using the operator $H+L$ and Eq. (9), that the values of the functions and derivatives on the boundaries of the sector are related by

$$\vec{F}(a_{n-1}) = \mathbf{r}_2^n\vec{F}'(a_n) - \mathbf{r}_1^n\vec{F}'(a_{n-1})$$

$$\vec{F}(a_n) = \mathbf{r}_4^n\vec{F}'(a_n) - \mathbf{r}_3^n\vec{F}'(a_{n-1}), \tag{11}$$

where the matrices of $\mathbf{r}_1^n$ to $\mathbf{r}_4^n$, called the sector R matrices, are given by

$$(r_1^n)_{ij} = \frac{1}{2}\sum_k \frac{g_{ik}(a_{n-1})g_{jk}(a_{n-1})}{E_k - \epsilon},$$

$$(r_2^n)_{ij} = \frac{1}{2}\sum_k \frac{g_{ik}(a_{n-1})g_{jk}(a_n)}{E_k - \epsilon},$$

$$(r_3^n)_{ij} = \frac{1}{2}\sum_k \frac{g_{ik}(a_n)g_{jk}(a_{n-1})}{E_k - \epsilon}, \quad (r_4^n)_{ij} = \frac{1}{2}\sum_k \frac{g_{ik}(a_n)g_{jk}(a_n)}{E_k - \epsilon}, \tag{12}$$

and

$$g_{\lambda k}(r) = \sum_j c_{j\lambda}^k \frac{f_j(r)}{r}. \tag{13}$$

In summary, knowing the eigenvalues and eigenvectors of Eq. (9), one can construct the sector R matrices $\mathbf{r}_1^n$ to $\mathbf{r}_4^n$ above, which, through Eqs. (11), relate the radial solutions and their derivatives on the boundaries of the sector. The R matrix relates the function to its derivative, i.e., $\vec{F}(a_n) = \mathbf{R}(a_n)\vec{F}'(a_n)$, and a simple manipulation of Eq. (11) yields the relationship between the R matrix on the inner and outer boundaries of the sector,

$$\mathbf{R}(a_n) = \mathbf{r}_4^n - \mathbf{r}_3^n[\mathbf{r}_1^n + \mathbf{R}(a_{n-1})]^{-1}\mathbf{r}_2^n, \tag{14}$$

where $\mathbf{R}(a_n)$ and $\mathbf{R}(a_{n-1})$ are represented in the same adiabatic basis set as the sector R matrices.

As the adiabatic basis changes from sector to sector, we need finally to change the basis representation of the R matrix. The matrix with elements

$$(T^{n-1,n})_{\lambda\lambda'} = \langle \phi_\lambda(r_a^{n-1};\theta,\phi)|\ \phi_{\lambda'}(r_a^n;\theta,\phi)\rangle \tag{15}$$

is thus constructed. One uses this transformation to change the basis representation of R, giving

$$\tilde{\mathbf{R}} = \overline{\mathbf{T}}^{n-1,n}\mathbf{R}\mathbf{T}^{n-1,n}, \tag{16}$$

where $\overline{\mathbf{T}}$ is the transpose of $\mathbf{T}$.

Starting with some initial R matrix, it can thus be propagated from sector to sector using Eqs. (14) and (16). Using the initial input R matrix given by Eq. (3), the propagation gives the final R matrix on the outer boundary in the asymptotic region at $r=b$, with the final R matrix being represented in the local adiabatic basis of the last sector.

Although it is possible to propagate the R matrix itself at each of the sector radii as described above, it is more practical and efficient to derive global sector R matrices ($\mathbf{R}_1$, $\mathbf{R}_2$, $\mathbf{R}_3$, and $\mathbf{R}_4$) relating the first and nth sectors [17], which can be built up sequentially using Eq. (11). One initially generalizes Eq. (11) to relate the values of the functions and derivatives on the boundaries of the first and nth sectors,

$$\vec{F}(a_1) = \mathbf{R}_2^n\vec{F}'(a_n) - \mathbf{R}_1^n\vec{F}'(a_1),$$

$$\vec{F}(a_n) = \mathbf{R}_4^n\vec{F}'(a_n) - \mathbf{R}_3^n\vec{F}'(a_1). \tag{17}$$

The operator relations for these global sector R matrices, including the change in basis, have been derived by Stechel *et al.* [17], and can be obtained by matching the wave function and its derivative on the boundaries between each of the n sectors. They are

$$\mathbf{R}_1^n = \mathbf{R}_1^{n-1} - \mathbf{R}_2^{n-1}\overline{\mathbf{T}}^{n-1,n}\mathbf{Z}^n\mathbf{T}^{n-1,n}\mathbf{R}_3^{n-1},$$

$$\mathbf{R}_2^n = \mathbf{R}_2^{n-1}\overline{\mathbf{T}}^{n-1,n}\mathbf{Z}^n\mathbf{r}_2^n,$$

$$\mathbf{R}_3^n = \mathbf{r}_3^n\mathbf{Z}^n\mathbf{T}^{n-1,n}\mathbf{R}_3^{n-1},$$

$$\mathbf{R}_4^n = \mathbf{r}_4^n - \mathbf{r}_3^n\mathbf{Z}^n\mathbf{r}_2^n, \tag{18}$$

where

$$\mathbf{Z}^n = (\mathbf{r}_1^n + \mathbf{T}^{n-1,n}\mathbf{R}_4^n\overline{\mathbf{T}}^{n-1,n})^{-1}.$$

In these equations, $\mathbf{R}_i^n$ are the global sector R matrices for all sectors up to n, $\mathbf{r}_i^n$ are the sector R matrices for sector n, and $\mathbf{T}^{n-1,n}$ is the transformation matrix between the adiabatic bases used in sectors $n-1$ and n. In an analogous way to Eq. (14) the global sector R matrices at the end of the propagation through all N sectors are used to relate the R matrix at $r=a$ to the R matrix at $r=b$,

$$\mathbf{R}(b) = \mathbf{R}_4^N - \mathbf{R}_3^N[\mathbf{R}_1^N + \mathbf{R}(a)]^{-1}\mathbf{R}_2^N. \tag{19}$$

Note that $\mathbf{R}_1^N$ to $\mathbf{R}_4^N$, determined from Eq. (18) above, are independent of which atom one uses, so that once they are calculated from the propagation then $\mathbf{R}(b)$ for a whole set of atoms can be evaluated at once using Eq. (19) by just using the appropriate quantum defects to calculate $\mathbf{R}(a)$ in Eq. (3). Hence, for given values of B, m, and π_z, the cross sections of all atoms of interest can be calculated simultaneously without the need for any additional propagations.

B. Asymptotic region

Having found the R matrix at $r=b$ by propagation, we must match this to the asymptotic solutions at $r=b$ to find the solution over all space. For large r, $r>b$, the magnetic field dominates. Since the motion in ρ is bounded $-1/r\rightarrow -1/z$, and the Hamiltonian in Eq. (1) is separable in cylindrical coordinates,

$$H = -\frac{1}{2}\frac{d^2}{dz^2} - \frac{1}{z} + H_L + O\left(\frac{1}{z^3}\right), \tag{20}$$

where H_L is the Hamiltonian for the Landau states,

$$H_L = -\frac{1}{2}\frac{1}{\rho}\frac{\partial}{\partial\rho}\left(\rho\frac{\partial}{\partial\rho}\right) + \frac{m^2}{2\rho^2} + \beta L_z + \frac{1}{2}\beta^2\rho^2. \tag{21}$$

H_L has eigenvalues $E_i^L=(2i+|m|+m+1)\beta$, $i=0,1,2\ldots$, and its eigenfunctions are the Landau states $\Phi_i(\rho,\phi)$ [1]. The asymptotic region $c\le z\le\infty$, $0\le\rho\le\infty$ with c less than the radius $r=b$ is therefore chosen to conform with the cylindrical symmetry of the problem. In this region, a set of j linearly independent solutions may be written, as is standard in scattering theory [11], in terms of the solutions of Eq. (20). These are a product of Landau states Φ_i and a linear combination of energy-normalized regular and irregular Coulomb functions s and c, in z, evaluated at an energy $\epsilon_i=\epsilon-E_i^L$, namely,

$$\Psi_{\epsilon j} = \sum_{ik}\Phi_i(\rho,\phi)[s_{ik}^{\epsilon_i}(z)\delta_{kj} + c_{ik}^{\epsilon_i}(z)K_{kj}]. \tag{22}$$

The constants K_{kj}, the reactance matrix or K matrix, are to be determined by the matching procedure.

The R matrix $\mathbf{R}(b)$, having been evaluated using Eq. (19), is now matched through a two-dimensional matching procedure to these asymptotic solutions on an arc at $r=b$ [8]. To perform this matching the integrals

$$\langle\phi_\lambda(b;\theta,\phi)|\Psi_{\epsilon j}\rangle = \int \phi_\lambda\Psi_{\epsilon j}d\Omega \tag{23}$$

must be evaluated, i.e., the asymptotic solutions must be projected onto the local adiabatic solutions on the radial arc at $r=b$. This is done by evaluating numerically the four matrices $\mathbf{P}$, $\mathbf{Q}$, $\mathbf{P}'$, $\mathbf{Q}'$ with elements

$$P_{\lambda j}(b) = \int (\phi_\lambda(b;\theta,\phi)\sum_i \Phi_i(\rho,\phi)s_{ij}(z))_{r=b}d\Omega,$$

$$Q_{\lambda j}(b) = \int (\phi_\lambda(b;\theta,\phi)\sum_i \Phi_i(\rho,\phi)c_{ij}(z))_{r=b}d\Omega,$$

$$P'_{\lambda j}(b) = \int (\phi_\lambda(b;\theta,\phi)\sum_i \Phi_i(\rho,\phi)s'_{ij}(z))_{r=b}d\Omega,$$

$$Q'_{\lambda j}(b) = \int (\phi_\lambda(b;\theta,\phi)\sum_i \Phi_i(\rho,\phi)c'_{ij}(z))_{r=b}d\Omega, \tag{24}$$

where the prime indicates the derivative with respect to z. This gives the regular and irregular components of the solu-

tions at $r=b$ and allows one to calculate the outer R matrix from the asymptotic region at $r=b$ in terms of K, the reactance matrix. Equating the inner and outer R matrices at $r=b$ gives

$$\mathbf{R} = [\mathbf{P} + (\mathbf{QK})][\mathbf{P}' + (\mathbf{Q}'\mathbf{K})]^{-1}. \tag{25}$$

Rearranging this expression gives us the equation for the K matrix,

$$\mathbf{K} = [(\mathbf{RQ}') - \mathbf{Q}]^{-1}[(\mathbf{RP}') - \mathbf{P}]. \tag{26}$$

Knowing **K**, we have the energy-normalized solution over all space and we can calculate both partial and total photoionization cross sections. However, we first describe how MQDT can be used to obtain **K** efficiently before showing how the dipole integrals and photoionization cross sections are calculated.

Multichannel quantum defect theory

For a given total energy ϵ there are two possibilities for the behavior of the Coulomb solutions in Eq. (22). If $\epsilon_i = \epsilon - E_i^L > 0$ the channel is open and the Coulomb functions oscillate at $r=b$ and all the way to infinity. If $\epsilon_i < 0$ then the channel is closed and the solutions must decay as $z \to \infty$. The physical **K** matrix therefore is a square matrix with the dimension of the number of open channels. However, with multichannel quantum defect theory one exploits the known analytic properties of the Coulomb functions to enforce the boundary conditions for the closed channels. For the closed channels there are two possible scenarios at $r=b$. Either the channel is strongly closed and is already exponentially small at $r=b$, or it is weakly closed, i.e., the Coulomb functions are still oscillating at $r=b$ before decaying at infinity. In MQDT, for a weakly closed channel, one instead uses Coulomb functions in Eq. (22) which do not decay at infinity, and one treats the channel as if it is open, enforcing the boundary condition at infinity analytically only in a final step [11]. Therefore the resonance structure due to these weakly closed channels can be calculated analytically. Hence the K matrix calculated by doing the matching using MQDT, denoted by $\mathcal{K}$, has dimension given by the number of open plus weakly closed channels. In general $\mathcal{K}$ has a slow dependence on energy as opposed to the rapid energy dependence present in **K**, because the Rydberg series of resonances converging on the Landau thresholds corresponding to the weakly closed channels have not as yet been included.

The open part of the actual physical reactance matrix K can be recovered from the matrix $\mathcal{K}$ by the formula [11]

$$\mathbf{K}_{oo} = \mathcal{K}_{oo} - \mathcal{K}_{oc}[\tan(\pi\nu) + \mathcal{K}_{cc}]^{-1}\mathcal{K}_{co}. \tag{27}$$

The o and c subscripts refer to the open and closed channels of $\mathcal{K}$ and the $\tan \pi\nu$'s form a diagonal matrix where the ν's are related to the energies ϵ_i by

$$\nu_i = \frac{1}{\sqrt{2|\epsilon_i|}}. \tag{28}$$

This way of obtaining the K matrix has two major advantages. First, it is much quicker computationally since $\mathcal{K}$ represents a reactance matrix with a lot of the resonance structure removed. Hence it varies much more slowly with energy than the full reactance matrix K. This allows one to calculate $\mathcal{K}$ on a coarse energy mesh with fairly large energy spacings. These $\mathcal{K}$'s can then be used to calculate K over an arbitrarily fine energy mesh using the analytic formula in Eq. (27). This allows the propagation stage to be performed at fewer energy points, ultimately speeding up the calculation enormously. The second major advantage of this approach is that the resonance structure converging to a particular Landau threshold can be identified by removing it from K. This is done by keeping open the relevant Landau channel in the evaluation of Eq. (27). By comparing a spectrum with all resonances converging on a particular Landau threshold removed with the full spectrum it is possible to determine which resonances converge to which thresholds [8,18]. This technique is demonstrated in Sec. IV.

C. Photoionization cross section

The photoionization cross section is given by

$$\sigma = 4\pi^2\alpha\omega|\langle\Psi_\epsilon^-|\vec{\epsilon}\cdot\vec{r}|\Psi_o\rangle|^2 \tag{29}$$

where α is the fine structure constant, ω the photon energy, $\vec{\epsilon}$ the polarization direction, Ψ_o the initial bound state, and Ψ_ϵ^- the energy-normalized "incoming" wave function [19]. There is a standard transformation to go from the K-matrix form given in (22) to the S matrix or incoming form Ψ_ϵ^- [11]. Once the K matrix and hence the asymptotic form are known from the matching, the photoionization cross section is evaluated by calculating the amplitude of the wave function near the origin, and hence the dipole integrals, as follows.

The incoming wave function solution on the inner boundary of the strong-mixing region ($r=a$) can be written as

$$\Psi_\epsilon^- = \sum_l F_l^-(a)Y_{lm}(\theta,\phi). \tag{30}$$

The wave function on the outer boundary of the strong-mixing region can be written as

$$\Psi_\epsilon^- = \sum_\lambda G_\lambda^-(b)\phi_\lambda(b;\theta,\phi), \tag{31}$$

where G_λ^- is the energy-normalized incoming asymptotic solution calculated from the matching procedure in Sec. II B. The radial solutions $\vec{F}^-$ and $\vec{G}^-$ are linked by the global sector R matrices as given in Eq. (17) so that

$$\vec{F}^-(a) = \mathbf{R}_2^N\vec{G}'^-(b) - \mathbf{R}_1^N\vec{F}'^-(a). \tag{32}$$

The radial solutions at $r=a$ can be written in terms of the field-free solutions **S** as $\vec{F}^- = \mathbf{S}\vec{A}^-$ from Eq. (2), where **S** is a diagonal matrix with elements

$$s_l^\epsilon(a) + c_l^\epsilon(a)\tan\pi\mu_l, \tag{33}$$

and $\vec{A}^-$ are the field- and energy-dependent amplitudes. Substitution into Eq. (32) yields the equation

$$(\mathbf{S} + \mathbf{R}_1^N\mathbf{S}')\vec{A}^- = \mathbf{R}_2^N\vec{G}'^-(b). \tag{34}$$

The coefficients $\vec{A}^-$ can therefore be evaluated by solving the above set of linear equations because $\vec{G}'^-(b)$ is known once

the K matrix is known. Using the coefficients $\vec{A}^-$, one can then simply calculate the dipole integrals in terms of the field-free dipole integrals multiplied by the appropriate components of $\vec{A}^-$, since the coefficients $\vec{A}^-$ are by definition the amplitudes that multiply the field-free solutions appropriate near the origin. For example, for excitation from the $1s$ state of hydrogen using linearly polarized light ($\Delta m=0$), only the $l=1$ component of the final state will be accessed. The photoionization cross section in this case is therefore given by

$$\sigma(\epsilon) = |A_1^-(\epsilon)|^2 \sigma_{B=0}. \tag{35}$$

where $\sigma_{B=0}$ is the field-free photoionization cross section for hydrogen.

III. COMPUTATIONAL DETAILS

The first point to address is the choice of the radii a and b. The inner radius must be taken larger than the core (~ 1 a.u.) for nonhydrogenic atoms, yet small enough that the diamagnetic term is still negligible compared to $-1/r$. For example, we took $a=200$ a.u. for laboratory strength fields. For the asymptotic radius b, extensive calculations show that it is surprisingly large, indicating that the long-range coupling due to the terms of $O(1/z^3)$ falls off very slowly. Based on our experience, we used the following empirical formula for an arbitrary field:

$$b = 700\left(\frac{10^{-3}}{\beta}\right)^{2/3}. \tag{36}$$

The number of sectors between $r=a$ and $r=b$ and their sizes are chosen in the following way. First one chooses the maximum energy to be used in the calculation, $\epsilon_{\max}$. The transformation matrix $(T^{n-1,n})_{\lambda\lambda'}$ between adiabatic functions evaluated at two radii r_a^{n-1} and r_a^n for consecutive sectors can be calculated using Eq. (15). If r_a^{n-1} was equal to r_a^n, $(T^{n-1,n})_{\lambda\lambda'}$ would be the identity matrix. As the distance $|r_a^{n-1}-r_a^n|$ increases, the corresponding adiabatic functions become more different. The effect this has on T is that the diagonal elements get smaller and the off-diagonal elements get bigger. The maximum sector size for the angular adiabatic basis is found by choosing a limit on how small any of the diagonal elements of T can become. Choosing a value of 0.5 for the smallest diagonal element restricts the size of each sector for a laboratory strength field to those shown in Fig. 2. One can see that for small and large r the adiabatic functions do not vary much with r, being close to spherical harmonics and Landau states, respectively, leading to large sector sizes. The intermediate range of r, where the avoided crossings in the potential curves shown in Fig. 1 are present, is where the angular functions are changing rapidly and one requires small sectors.

The radial basis sector widths are chosen by comparison with the local wavelength of the Coulomb functions, namely,

$$\text{Radial sector size} = \frac{\text{const}}{[2(\epsilon_{\max}+1/r)]^{1/2}}. \tag{37}$$

If a radial basis of ten Legendre polynomials is taken, it is found that const=6.0 is sufficient to produce an accurate description of the wave function [15]. For the maximum energy used, the sectors resulting from this criterion are also shown in Fig. 2. There are therefore two criteria for choosing the sector sizes; one from the radial basis and one from the angular basis. The smaller value of these two determines the actual sector sizes, and these are also shown in Fig. 2.

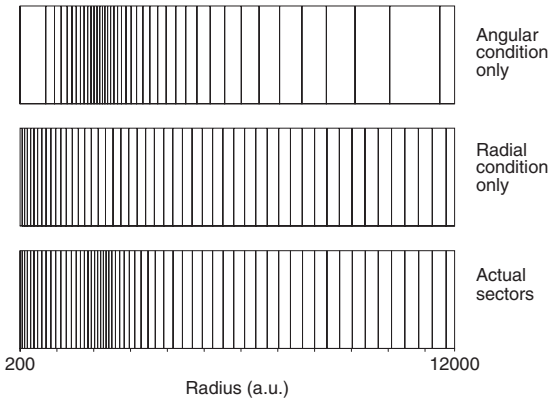

FIG. 2. Sector radii obtained using the angular condition only, the radial condition only, and both conditions as described in the text. The first and last sector radii are 200 and 12 000 a.u., respectively. The magnetic field strength is 6 T.

The adiabatic functions $\phi_\lambda(r_a^n;\theta,\phi)$ are obtained by diagonalizing the adiabatic Hamiltonian H_{ad} in a basis of spherical harmonics. The number of spherical harmonics used must ensure that the functions $\phi_\lambda(r_a^n;\theta,\phi)$ are properly converged. At the matching radius $r=b$, the ratio between the diamagnetic term and the potential term in H_{ad} will be at its greatest. It is therefore at this radius that the largest number of spherical harmonics will be required, because it is here that the adiabatic functions will have their greatest degree of cylindrical symmetry. We choose the number of l's so that the eigenvalue corresponding to the second closed channel at $r=b$ for an energy $\epsilon_{\max}$ is accurate to 0.5%. It has been verified that this is sufficient to give convergence in the final cross section.

When the R matrix is propagated from $r=a \rightarrow r=b$, it is necessary to retain, within any one sector, all of the locally open channels plus a few of the locally closed ones. The number of closed channels required is directly related to the threshold value on the adiabatic angular functions used to determine the sector sizes. The number of closed channels needed, however, is constant for all of the sectors. For a given energy ϵ, because the number of locally open channels changes with radius (see Fig. 1), the total number of channels retained in any one sector varies. Because it is very difficult to include a channel halfway through the propagation, the number of channels retained in a sector is found by the following method. First, the maximum number of open channels retained for a given $\epsilon_{\max}$ in any one sector is found, and this sector is labeled k. In every sector up to and including k the number of channels retained is this maximum number of open channels plus the number of extra closed channels. After sector k the number of channels retained is the number of locally open channels plus the number of closed channels. The redundant channels in the global sector R ma-

TABLE I. Number of open channels and total number of channels used in each sector of the propagation for a magnetic field strength of 470 T. Two extra closed channels are retained in each sector.

Outer sector radius (a.u.)	No. of local open channels	No. of channels used
23.41	3	8
43.94	3	8
72.05	4	8
108.04	5	8
141.02	6	8
189.01	4	6
247.23	3	5
313.78	2	4
388.78	1	3
472.01	1	3
563.75	1	3
663.93	1	3
700.00	1	3

trices are removed for any given energy ϵ by a simple truncation as it is required during the propagation stage. Essentially, once the saddle point of the adiabatic curves (see Fig. 1) is passed, the number of channels retained in the *R*-matrix propagation can be reduced. An example of the number of channels retained in a program run for a magnetic field strength 470 T is shown in Table I, showing that from about 190 a.u. on the number of channels propagated decreases with increasing r.

The number of channels needed to match the R matrix to asymptotic solutions in order to obtain the $\mathcal{K}$ matrix was checked for each spectrum to ensure convergence. Once the $\mathcal{K}$ matrix was obtained, however, the number of channels needed for the calculation of the cross section was reduced to the number of open channels plus the number of weakly closed channels. Weakly closed channels were taken to be those that were within an energy (in a.u.) of $1/b$ of their corresponding Landau energy.

The cross section is obtained over a coarse mesh of energies initially and then MQDT is used to calculate the cross section over an arbitrarily small energy range. The convergence of the cross sections was tested by varying the inner and outer radii, a and b, and the other parameters in the calculations.

IV. PHOTOIONIZATION CROSS SECTIONS FOR LABORATORY STRENGTH FIELDS

Calculations at laboratory strength fields are the most demanding numerically as the radial distances over which one needs to propagate the R matrix are large. The number of channels needed in the calculation can also become quite large. We focus on the photoinization spectrum of lithium in a magnetic field of 6.1143 T ($\beta=1.3\times10^{-5}$), where experimental data exist (Iu *et al.* [10]). Lithium is excited from the

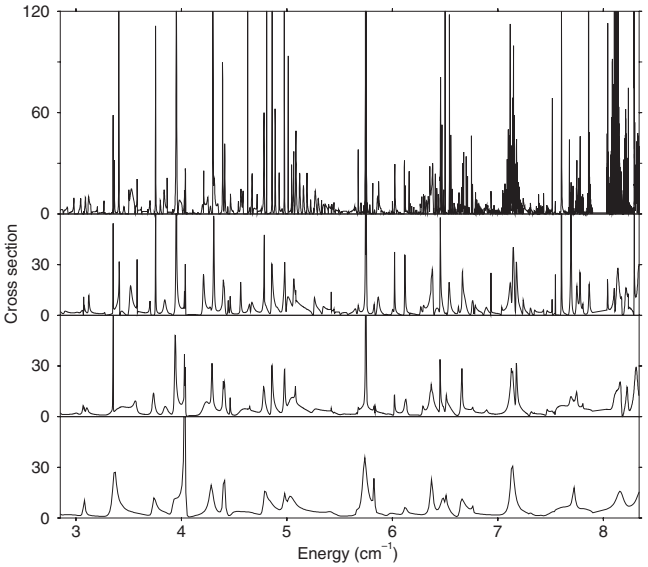

FIG. 3. Photoionization cross section of lithium in arbitrary units versus the energy in wave numbers measured relative to the field-free ionization threshold. Excitation is from the $3s$ state in a field strength of 6.1143 T using linearly polarized light. The final state has $m=0$ and $\pi_z=-1$. The top panel shows the full spectrum and the second, third, and fourth panels show the spectrum with all the resonances converging on the nearest, second-nearest, and third-nearest thresholds removed using multichannel quantum defect theory.

$3s$ state using linearly polarized light, giving a final state with $m=0$ and $\pi_z=-1$ or odd z parity. We show in Fig. 3 the calculated spectrum between the photoionization threshold (i.e., $i=0$ or the first Landau level) and the second Landau level or threshold, $i=1$.

The only significant quantum defect is for $l=1$, $\mu_p=0.053$. (The $l=0$ continuum partial wave does not play any role for excitation from s states.) The photoionization cross section is given in arbitrary units but it can be put on an absolute scale if the field-free cross section is known. The radius a is 200 and $b=12\,600$. The adiabatic matrix threshold was taken to be 0.1. Together with an $\epsilon_{\max}$ of 3.9×10^{-5} a.u., this gives the number of sectors as 64. The maximum number of locally open adiabatic channels is 27, and taking 13 extra closed channels the maximum number of channels overall is 40; hence the maximum size matrix to be diagonalized is 400 since there are ten radial basis functions per sector. The cross section is calculated over a coarse mesh at 400 energy points between the thresholds. The full spectrum is then calculated semianalytically using MQDT and Eq. (27) with over 10 000 energy points. The spectrum obtained from this calculation is displayed in the top panel of Fig. 3 showing the complete resonance structure between the thresholds. MQDT can also be used to examine the resonance structure by keeping individual weakly closed channels open, i.e., by not enforcing the closed channel conditions asymptotically. For a single threshold this is equivalent to a Gailitis average [11,20] over the resonances converging to that threshold. For several thresholds this is a type of generalized Gailitis average over the resonance structure, and

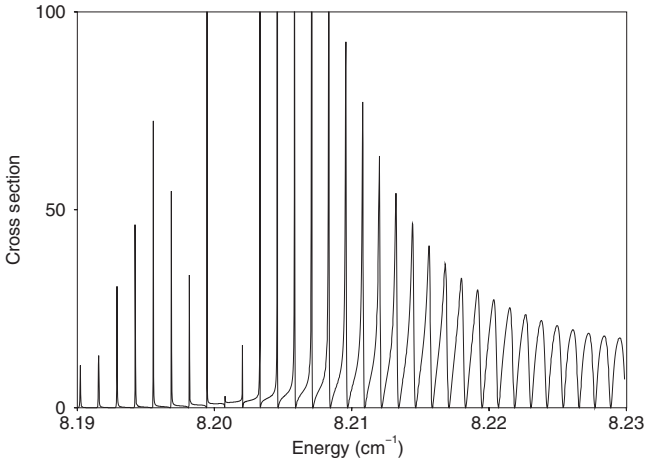

FIG. 4. Photoionization cross section of lithium in arbitrary units over a very small energy range just below the first excited Landau threshold. This demonstrates the arbitrary resolution of the theoretical technique.

would be similar to convoluting the actual spectrum with a Gaussian of a certain width [18]. The differences between the first and second panels allows one to identify the perturbed resonances which converge to the second Landau level or threshold, $i=1$. The third panel in Fig. 3 has resonances converging on the next two thresholds removed ($i=1$ and 2) and the final panel has resonances converging to the $i=3$ threshold also removed. Some of the remaining modulations may be resonances converging on higher Landau levels, but cannot be removed because the wave functions of these resonances are completely contained within the radius $b=12\,600$. A lower matching radius would be required to further reduce the spectrum. Note that the final panel contains only about 20 resonances, compared to the very large number in the first panel, indicating that much of the complex resonance structure is due to several Rydberg series interacting with a finite number of short-range perturbers.

In addition to helping in the analysis of the spectrum, MQDT allows one to calculate the resonance structure to an arbitrarily small resolution. This is demonstrated in Fig. 4 where an enlargement of the spectrum in a very small energy region just below the first excited Landau level is shown.

However, the real power of the combination of R-matrix propagation with adiabatic bases can be seen in Fig. 5, where we calculate the photoionization cross section over an extended energy region covering over six Landau thresholds from the ionization threshold. Because the number of open channels increases with energy, the sizes of the matrices to be diagonalized are slightly larger. The total number of sectors increases also but, even for the highest energy, the number of channels did not exceed 50, so that the largest matrices that need to be diagonalized are of the order of 500. The cross section was calculated on a coarse energy grid of 500 points over each of the thresholds before applying MQDT. The method scales in a reasonable way, thus allowing one to calculate the photoionization cross section of an atom over a large energy range above the ionization threshold.

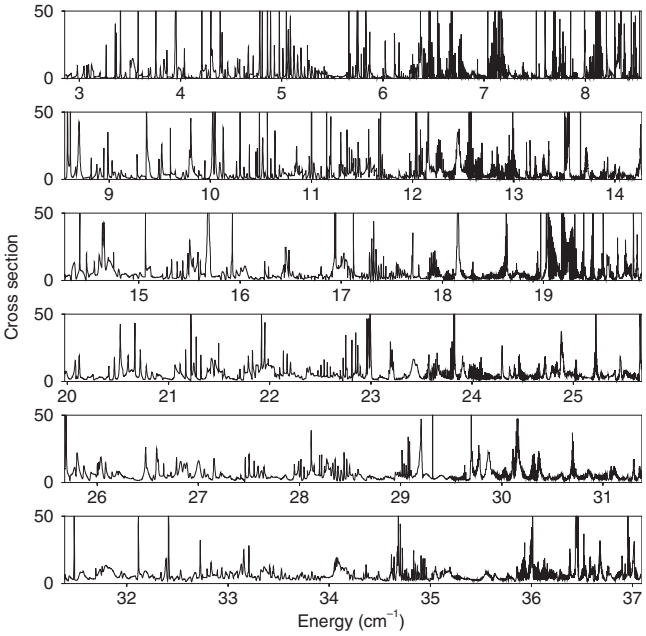

FIG. 5. The extension of the photoionization spectrum of lithium in arbitrary units in a magnetic field of 6.1143 T, shown in Fig. 3, to an energy range covering over six Landau thresholds. Each panel shows the spectrum over one Landau threshold.

V. PHOTOIONIZATION CROSS SECTIONS FOR ASTROPHYSICAL STRENGTH FIELDS

Photoexcitation and photoionization cross sections of light elements such as hydrogen and helium are important in understanding the properties of white dwarf and neutron stars [2]. The method detailed in Sec. II can equally well be applied to atoms in astrophysical strength magnetic fields. In fact, the computation is much easier in this case compared to

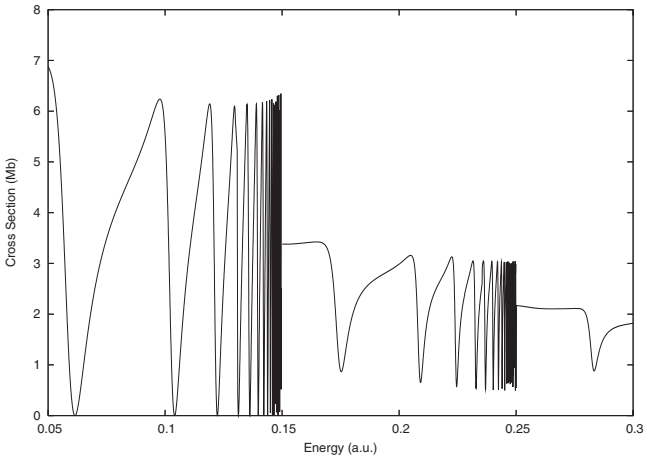

FIG. 6. Photoionization cross section of hydrogen in megabarns versus the energy in a.u. measured relative to the field-free ionization threshold. Excitation is from the $1s$ state in a field strength of 23 500 T using linearly polarized light. The final state is $m=0$ and $\pi_z=-1$. The energy range covers the first two Landau thresholds.

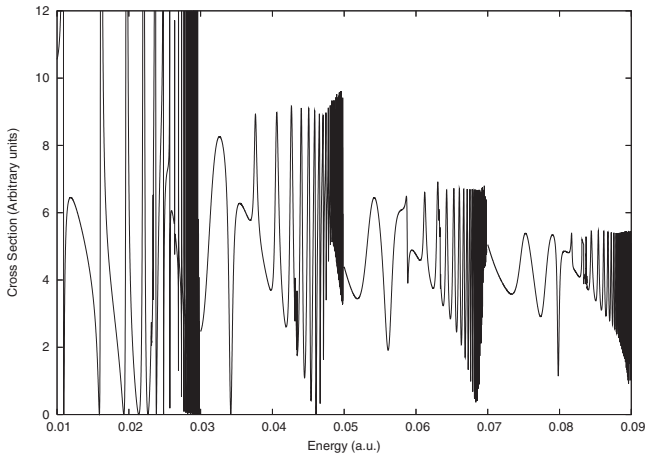

FIG. 7. Photoionization cross section of helium in arbitrary units versus the energy measured relative to the field-free ionization threshold. Excitation is from the ground state in a field strength of 4700 T using linearly polarized light.

laboratory strength fields as the radius b is much smaller and the number of channels and sectors is smaller too. We give just two examples to illustrate the point. We first consider the photoionization spectrum of hydrogen from the ground state using linearly polarized light in a field of 23 500 T ($\beta=0.05$ a.u.). (See Fig. 6.) The radius a was 1 a.u. and $b=50$, the number of sectors used was 20, and up to ten channels were used in the propagation. This spectrum has also been calculated using the complex coordinate method [6,21]. Excellent agreement is found between the two methods away from the energy region near the ionization thresholds. As the complex coordinate method uses a finite basis it cannot represent all of the Rydberg structure just below the ionization thresholds.

The second example is the photoionization spectrum of helium from the ground state in a field of 4700 T ($\beta=0.0001$ a.u.). The only significant quantum defect is for $l=1$, $\mu_p=-0.012$. (The $l=0$ continuum partial wave will play a role only for excitation from the $1s2p$ state.) The radius a was 5 a.u. and $b=150$, the number of sectors used was 20, and a maximum of 12 channels were used in the propagation. Resonances converging to the first four excited Landau thresholds are shown in Fig. 7. The resonance structure is that of strongly perturbed Rydberg resonances converging to the individual thresholds.

The spectra in both cases, when calculated over an extended energy range, repeat the patterns shown in Figs. 6 and 7.

VI. CONCLUSIONS

We have presented a detailed description of a method to evaluate the photoionization cross section of an atom in an external magnetic field. By combining *R*-matrix propagation with local adiabatic bases, we have shown that is possible to calculate the cross section over an extended energy range for a range of field strengths. We have calculated cross sections for a range of atoms in both laboratory and astrophysical field strengths to illustrate the generality of the method. In addition, for given values of B, m, and π_z, the spectra of all atoms of interest can be calculated without the need for any additional propagations. By using MQDT one is able to calculate quickly all of the resonances in the spectrum and to analyze some of their main characteristics. Partial cross sections to individual Landau levels are evaluated when calculating the total cross section, enabling one to calculate their distributions. The method can be used to calculate the large amounts of data needed for such problems as stellar opacities or for calculating recombination rates at low temperatures for an atom in a magnetic field.

ACKNOWLEDGMENT

We thank Dr. I. Moser for useful discussions.

APPENDIX

In constructing the matrix representation of the Hamiltonian plus Bloch operator in each sector one has to construct matrices for the operators

$$-\frac{1}{2}\frac{d^2}{dr^2}+\frac{l(l+1)}{2r^2}-\frac{1}{r} \tag{A1}$$

and r^2 with the radial basis set of shifted Legendre polynomials. For an arbitrary sector with inner radius $r=a$ and outer radius $r=b$, the coordinate r can be rescaled to the coordinate u such that

$$u=\frac{2}{b-a}\left[r-\left(\frac{b+a}{2}\right)\right]. \tag{A2}$$

The limits of the integrals in r over the limited range $a\rightarrow b$ therefore become $-1\rightarrow 1$ in the coordinate u. The orthogonal radial functions are thus

$$f_n(r)=\sqrt{\frac{2n-1}{b-a}}P_{n-1}(u), \tag{A3}$$

where P_n is the Legendre polynomial of order n. The kinetic term can be evaluated by integration by parts and by using the relation ([22], p. 282)

$$\int_{-1}^{+1}\frac{dP_n(u)}{du}\frac{dP_m(u)}{du}du=\begin{cases}n(n+1) & \text{if } m-n \text{ even},\\ 0 & \text{if } m-n \text{ odd},\end{cases} \tag{A4}$$

for $m\geq n$, or

$$\frac{1}{2}\int_a^b\frac{df_n}{dr}\frac{df_m}{dr}dr=\begin{cases}\frac{1}{2}\frac{\sqrt{(2n-1)(2m-1)}}{(b-a)^2}n(n-1) & \text{if } m-n \text{ even},\\ 0 & \text{if } m-n \text{ odd},\end{cases} \tag{A5}$$

where $m\geq n$.

The potential term I_{nm} is given by

$$I_{nm} = \int_a^b f_n(r)\left(-\frac{1}{r}\right)f_m(r)dr = \frac{\sqrt{(2n-1)(2m-1)}}{b-a}(-1) \times \int_{-1}^{+1} \frac{P_{n-1}(u)P_{m-1}(u)}{u+(b+a)/(b-a)}du. \quad \text{(A6)}$$

Using the relation

$$\int_{-1}^{+1} \frac{P_n(x)P_m(x)}{z-x}dx = 2P_n(z)Q_m(z), \quad \text{(A7)}$$

where $m \geq n$ and $Q_m(z)$ is a Legendre function of the second kind [22], the potential term becomes

$$I_{nm} = \frac{\sqrt{(2n-1)(2m-1)}}{b-a}2P_{n-1}\left(-\frac{(b+a)}{b-a}\right)Q_{m-1}\left(-\frac{(b+a)}{b-a}\right). \quad \text{(A8)}$$

Since

$$P_n(-z) = (-1)^n P_n(z),$$

$$Q_n(-z) = (-1)^{n+1} Q_n(z), \quad \text{(A9)}$$

one gets finally

$$I_{nm} = \frac{\sqrt{(2n-1)(2m-1)}}{b-a}2(-1)^{n+m+1} \times P_{n-1}\left(\frac{b+a}{b-a}\right)Q_{m-1}\left(\frac{b+a}{b-a}\right). \quad \text{(A10)}$$

The centrifugal term requires the integrals J_{nm},

$$J_{nm} = \int_a^b f_n(r)\frac{1}{r^2}f_m(r)dr = \frac{\sqrt{(2n-1)(2m-1)}}{(b-a)^2}\int_{-1}^{+1} \frac{P_{n-1}(u)P_{m-1}(u)}{[u+(b+a)/(b-a)]^2}du. \quad \text{(A11)}$$

The integral in this equation can be evaluated by differentiating Eq. (A7) to obtain

$$\int_{-1}^{+1} \frac{P_n(x)P_m(x)}{(z-x)^2} = \frac{-2}{z^2-1}[(n+1)P_{n+1}(z)Q_m(z) + (m+1)P_n(z)Q_{m+1}(z) + (n+m+2)zP_n(z)Q_m(z)], \quad \text{(A12)}$$

where the following relations have been used:

$$(z^2-1)\frac{dP_n(z)}{dz} = (n+1)P_{n+1}(z) - (n+1)zP_n(z),$$

$$(z^2-1)\frac{dQ_m(z)}{dz} = (m+1)Q_{m+1}(z) - (m+1)zQ_m(z). \quad \text{(A13)}$$

Substituting the appropriate value for z and using the relations in Eq. (A9) the final result is

$$J_{nm} = \frac{\sqrt{(2n-1)(2m-1)}}{(b-a)^2}\frac{(-2)}{c^2-1}(-1)^{n+m}[nP_n(c)Q_{m-1}(c) + mP_{n-1}(c)Q_m(c) - c(n+m)P_{n-1}(c)Q_{m-1}(c)], \quad \text{(A14)}$$

where

$$c = \frac{b+a}{b-a}. \quad \text{(A15)}$$

To evaluate the integral involving r^2, the recurrence relation

$$(2n+1)uP_n(u) = (n+1)P_{n+1}(u) + nP_{n-1}(u) \quad \text{(A16)}$$

is used. This yields

$$\int_a^b f_n(r)r^2 f_m(r)dr = \frac{(b-a)^2}{4}\left[\frac{n(n+1)}{(2n+1)\sqrt{2n-1}\sqrt{2n-3}}\delta_{mn+2} + \frac{2cn}{\sqrt{2n-1}\sqrt{2n+1}}\delta_{mn+1} + \left(c^2 + \frac{n^2}{(2n-1)(2n+1)} + \frac{(n-1)^2}{(2n-1)(2n-3)}\right)\delta_{nm} + \frac{2c(n-1)}{\sqrt{2n-1}\sqrt{2n-3}}\delta_{mn-1} + \frac{(n-1)(n-2)}{(2n-3)\sqrt{2n-1}\sqrt{2n-5}}\delta_{mn-2}\right]. \quad \text{(A17)}$$

To evaluate Eq. (A10) and Eq. (A14) the functions $P_n(c)$ and $Q_n(c)$ must be calculated. To calculate the Legendre polynomials $P_n(c)$, the standard recurrence relation

$$P_{n+1}(c) = \frac{(2n+1)c}{n+1}P_n(c) - \frac{n}{n+1}P_{n-1}(c) \quad \text{(A18)}$$

is used, where the first two Legendre polynomials are given by $P_0(c)=1$ and $P_1(c)=c$. The method required to calculate $Q_n(c)$ depends on the value c. For $c<1$ the same recurrence relation as Eq. (A18) can be used with $Q_0(c)=\frac{1}{2}\ln[(c+1)/(c-1)]$ and $Q_1(c)=(c/2)\ln[(c+1)/(c-1)]-1$. For $c>1$ the recurrence relation in Eq. (A18) should only be used for decreasing values of n. The first two values can be evaluated using the expression

$$Q_n(c) = \frac{1}{2} P_n(c) \ln\left(\frac{1+c}{1-c}\right) - W_{n-1}(c), \tag{A19}$$

where

$$\begin{aligned} W_{n-1}(c) &= \frac{2n-1}{1(n)} P_{n-1}(c) + \frac{2n-5}{3(n-1)} P_{n-3}(c) \\ &\quad + \frac{2n-9}{5(n-2)} P_{n-5}(c) + \cdots \\ &= \sum_{m=1}^{n} \frac{1}{m} P_{m-1}(x) P_{n-m}(x). \end{aligned} \tag{A20}$$

The first values could also be calculated using hypergeometric functions via

$$Q_n(c) = \frac{\pi^{1/2}}{2^{n+1}} \frac{\Gamma(n+1)}{\Gamma\left(n+\frac{3}{2}\right)} \frac{1}{c^{n+1}} F\left(1 + \frac{n}{2}, \frac{1}{2} + \frac{n}{2}; n + \frac{3}{2}; \frac{1}{c^2}\right) \tag{A21}$$

for $|c| > 1$; however, in the calculations described in this paper the expression in Eq. (A19) was used. The Legendre functions of the second kind can therefore be evaluated using the recurrence relation

$$Q_n(c) = \frac{n+2}{n+1} Q_{n+2}(c) - \frac{2n+3}{n+1} c Q_{n+1}(c). \tag{A22}$$

[1] S. Gaziorowicz, *Quantum Physics* (John Wiley, New York, 2003).

[2] H. Ruder, G. Wunner, H. Herold, and F. Geyer, *Atoms in Strong Magnetic Fields* (Springer-Verlag, Berlin, 1994).

[3] *Atoms and Molecules in Strong External Fields*, edited by P. Schmelcher and W. Schweizer (Plenum Press, New York, 1998).

[4] M. C. Gutzwiller, *Chaos in Classical and Quantum Mechanics* (Springer-Verlag, New York, 1991).

[5] O.-A. Al-Hujaj and P. Schmelcher, Phys. Rev. A **70**, 023411 (2004) and references therein.

[6] D. Delande, A. Bommier, and J. C. Gay, Phys. Rev. Lett. **66**, 141 (1991); M. H. Halley, D. Delande, and K. T. Taylor, J. Phys. B **26**, 1775 (1993).

[7] P. F. O'Mahony and F. Mota-Furtado, Comments At. Mol. Phys. **25**, 309 (1991).

[8] P. F. O'Mahony and F. Mota-Furtado, Phys. Rev. Lett. **67**, 2283 (1991); AIP Conf. Proc. **275**, 449 (1993).

[9] S. Watanabe and H. A. Komine, Phys. Rev. Lett. **67**, 3227 (1991).

[10] C. H. Iu, G. R. Welch, M. M. Kash, D. Kleppner, D. Delande, and J. C. Gay, Phys. Rev. Lett. **66**, 145 (1991).

[11] M. J. Seaton, Rep. Prog. Phys. **46**, 167 (1983).

[12] P. G. Burke and W. D. Robb, Adv. At. Mol. Phys. **11**, 143 (1975).

[13] M. J. Seaton, Comput. Phys. Commun. **146**, 254 (2002).

[14] J. C. Light and R. B. Walker, J. Chem. Phys. **65**, 4272 (1976).

[15] K. L. Baluja, P. G. Burke, and L. A. Morgan, Comput. Phys. Commun. **27**, 299 (1982).

[16] C. Bloch, Nucl. Phys. **4**, 503 (1957).

[17] E. B. Stechel, R. B. Walker, and J. C. Light, J. Chem. Phys. **69**, 3518 (1978).

[18] Q. Wang and C. H. Greene, Phys. Rev. A **44**, 7448 (1991).

[19] I. I. Sobelman, *Atomic Spectra and Radiative Transitions* (Springer-Verlag, Berlin, 1992).

[20] M. Gailitis, Sov. Phys. JETP **17**, 1328 (1963).

[21] L. B. Zhao and P. C. Stancil, Phys. Rev. A **74**, 055401 (2006).

[22] E. T. Copson, *Introduction to the Theory of Functions of a Complex Variable* (Oxford University Press, Oxford, 1970).